Journal of Nuclear Materials 408 (2011) 54–60

Contents lists available at ScienceDirect

Journal of Nuclear Materials

journal homepage: www.elsevier.com/locate/jnucmat

Novel insights in the study of water penetration into polycrystalline UO_2 by secondary ion mass spectrometry

Ilaria Marchetti, Fabio Belloni *, Jerome Himbert, Paul Carbol, Thomas Fanghänel

European Commission, Joint Research Centre, Institute for Transuranium Elements, P.O. Box 2340, D-76125 Karlsruhe, Germany

ARTICLE INFO

Article history:
Received 25 February 2010
Accepted 31 October 2010

ABSTRACT

Oxygen and water species (e.g., OH^-, H_2O) diffusion in polycrystalline UO_2 are key parameters to investigate in order to predict spent fuel behaviour in a final repository in the event of exposure to groundwater. In this work, ^{18}O tracer diffusion is evaluated by means of secondary ion mass spectrometry on a UO_2 pellet exposed to ^{18}O-labelled water at room temperature for 3 months. Depth profiling up to 22 μm beneath the pellet surface clearly indicates a combination of oxygen diffusion into the UO_2 lattice and water species diffusion along grain boundaries, behaving as high-diffusivity-paths. The relevant coefficients have been estimated around 1.4×10^{-24} m^2 s^{-1} for lattice diffusion and around 2.3×10^{-16} m^2 s^{-1} for grain boundary diffusion.

1. Introduction

Uranium dioxide, as the main component of conventional nuclear fuel, has been for long time under close chemical investigation. In particular, the interaction of water with polycrystalline UO_2 has to be characterized as it promotes the mobilization of radionuclides in the event of exposure of spent fuel to groundwater in a final repository. Preferential dissolution of grain boundaries rather than matrix dissolution could cause a rapid increase of the fuel surface area exposed to groundwater, and consequently of the fraction of inventory becoming available for dissolution. In the long term, this may also decrease the overall mechanical stability of the spent fuel pellet.

Here, we report experiments that aim at understanding the mechanisms of water penetration into polycrystalline UO_2 under conditions relevant to final disposal of spent nuclear fuel in a geological repository. In this preliminary phase, the study has been focused on unirradiated UO_2 with well defined grain size and morphology, but the observed mechanisms of water penetration may be extended to irradiated fuel and other polycrystalline waste form materials [1] with similar composition and morphology.

The key parameters to evaluate are the diffusion coefficients of oxygen in the UO_2 lattice and of the species that may be responsible for the transport of oxygen along the grain boundaries (presumably O^{2-}, H_2O, OH^- or more complex hydrogen–oxygen species [2,3]). For oxygen, several attempts to estimate the coefficients for both chemical diffusion and self-diffusion (i.e., diffusion in presence or absence of a concentration gradient, respectively) have been made, mostly with indirect approaches, e.g., measurements of electrical conductivity after reduction of oxidised samples [4], thermogravimetry following steam oxidation [5], or gas–solid isotopic exchange coupled with sample sectioning [6]. As well as the problem of the inconsistency in the reported values, the applicability of these data to the prediction of oxidation kinetics in final disposal scenarios is further constrained by the fact that all experiments have been performed in temperature ranges between 600 and 1800 K, whereas in a final repository the temperature can be expected to be in the range 290–370 K [7]. Considering the exponential dependence of the diffusion coefficient on temperature, it may not be sufficiently reliable to extrapolate the Arrhenius behaviour to such low temperatures.

Secondary ion mass spectrometry (SIMS) offers the most reliable alternative to the classical radiotracer methods used for diffusion studies, granting high sensitivities and high depth resolution. SIMS depth profiling of the $^{18}O/^{16}O$ isotopic ratio into polycrystalline UO_2, using $H_2{}^{18}O$ as a tracer, provides a *direct* observation of the phenomenon, allowing the experiments to be performed at room temperature. A further advantage is the possibility of discriminating between short and long-range diffusion simply by adapting the sputtering rate. In spite of this, even the SIMS study of diffusion by Sabioni et al. [8] preferentially focuses on experiments carried out at high temperatures, probably to reduce their duration. In fact, that work involved gas–solid isotopic exchange in ^{18}O-labelled water vapour at 880–1000 K. In the present study instead, SIMS depth profiling was applied – for the first time to our knowledge – to trace the diffusion of oxygen and water after static leaching of polycrystalline UO_2 in ^{18}O-labelled water at room temperature. The preliminary results reported here have shown to be promising and similar studies are underway on different matrices, such as UO_2 single crystal, simulated and reactor-irradiated

* Corresponding author. Tel.: +49 (0) 7247 951 116; fax: +49 (0) 7247 951 99116.
E-mail address: fabio.belloni@ec.europa.eu (F. Belloni).

0022-3115/$ - see front matter © 2010 Elsevier B.V. All rights reserved.
doi:10.1016/j.jnucmat.2010.10.065

fuel. This will allow us to outline a more comprehensive picture of the impact of grain boundaries, microcracks and burnup-induced microstructures on water intrusion.

2. Material and methods

A commercial natural UO_2 pellet (Siemens AG, 0.72 wt.% ^{235}U, diameter 8 mm) was cut to obtain two 3 mm thick discs with parallel faces (1.71 g). The thermally etched grains are visible in the picture in Fig. 1 and a grain size distribution has been measured on a set of SEM images resulting in a mean value of 9.4 μm. The density of the UO_2 pellets has been measured by Archimedes' method resulting in a value of 96% of the theoretical density [9].

After the cut, the discs were polished in several steps until surface roughness was reduced to a few tens nm. The root-mean-squared roughness, S_{RMS}, typically ranged from 10 nm to 70 nm, as measured by atomic force microscopy (Veeco – Digital Instruments, Dimension 3100; WSxM Scanning Probe Microscopy Software [10]) on areas comparable in size to the SIMS field of analysis; a roughness factor (i.e., rugosity) [11] of about 1.02 was calculated, whereas the average slope of surface profiles was typically found below 0.1 nm/μm. The discs were finally annealed in an oven (6 h at 1700 K, 1 l/min 96% Ar/4% H_2 flow). One of them was then simply stored under vacuum to be analysed as a blank, while the other was placed at the bottom of a glass vial with 2 ml ^{18}O-labelled water (Chemotrade, 96 at.% $H_2{}^{18}O$). The vial was maintained at room temperature in an air atmosphere for the length of the corrosion experiment. After 3 months the UO_2 disc was extracted from the leachant, dried in air and mounted in a sample holder so that the surface could be analysed by means of SIMS (Cameca, IMS-622).

For the SIMS analysis, a 15 keV Cs^+ primary beam was used for both imaging and depth profiling, while negative secondary ions were detected. No metal coating of the surface or electron flood gun was necessary to compensate for charging effects.

Ion maps of the pellet surface were recorded for $^{18}O^-$ and $^{238}U^{16}O_2{}^-$ using a primary current of about 0.2 nA over a $70 \times 70\ \mu m^2$ area. Typical example of SIMS images are shown in Fig. 2.

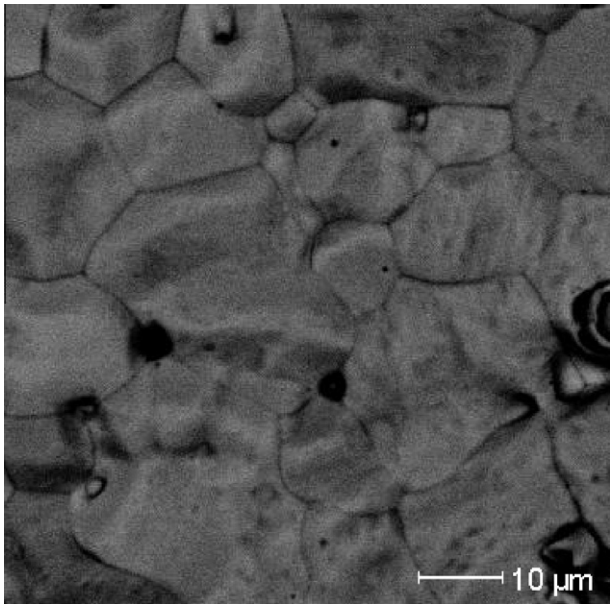

Fig. 1. Backscattered electron image of a polycrystalline UO_2 pellet.

Depth profiles were acquired starting with a primary intensity of about 2 nA to probe the short-range diffusion depth, and proceeding with the application of about 50 nA for the long-range depth profile. The beam raster covered a $150 \times 150\ \mu m^2$ area, while the diameter of the analysed area was ~33 μm, so that the secondary ions were collected only from the central part of the crater. In order to limit the impact of the isobaric interference of $^{17}OH^-$ (18.0068 amu) and $H_2{}^{16}O^-$ (18.0146 amu) on $^{18}O^-$ (17.9992 amu), the mass resolution $M/\Delta M$ of the spectrometer was set around 1500. Nevertheless, an insignificant intensity was detected for the cumulative signal of the species $^{17}OH^-$ and $H_2{}^{16}O^-$, as shown in the raw SIMS depth profiles in Fig. 3. Due to their low counting rate, $^{18}OH^-$ and $H_2{}^{18}O^-$ signals (not shown) were not systematically acquired; in this study, only $^{18}O^-$ has been taken into account as the diffusion-tracing secondary species.

Calibration of the depth scale of the SIMS profiles vs. the sputtering time was performed through the determination of the sputtering rate of the material, accomplished by producing several craters at different sputtering times. The depth of every crater was measured by means of a high resolution profilometer (Veeco, Dektak 8000). A typical crater profile is shown in Fig. 4a. The depth Λ of a crater is linearly related to the intensity of the primary beam I_p and the time of analysis t_s according to:

$$\Lambda = K I_p t_s \tag{1}$$

where the proportionality constant K is the sputtering rate per unit current. Plotting the depth of the craters vs. the product of the sputtering time and the primary intensity, the slope of the fitting linear function, as shown in Fig. 4b, was found to be $K = 0.016 \pm 0.001$ nm nA^{-1} s^{-1} (2σ standard error). This factor was used to convert the sputtering time to depth. Attention is drawn to the fact that the two points around $I_p\ t_s \approx 366$ nA h (obtained with $I_{p,1} = 26.7$ nA, $t_{s,1} = 13.8$ h and $I_{p,2} = 52.1$ nA, $t_{s,2} = 7.0$ h, respectively) show very good reciprocity of the two different parameters I_p and t_s. The possible difference in the sputtering rate due to the different crystallographic orientation [12] of the grains composing the UO_2 pellet is averaged out thanks to the fact that every measurement involves a statistically significant number of grains, given the typical raster area ($150 \times 150\ \mu m^2$), the range of crater depths (up to 33 μm) and the average diameter of the grains (9.4 μm). The sputtering rate so determined becomes, as a consequence, the more reliable the deeper the crater is.

The ^{18}O relative isotopic abundance, c, averaged over the surface of the analysed area, was calculated according to the relation:

$$c = \frac{I(^{18}O^-)}{I(^{18}O^-) + I(^{16}O^-)} \tag{2}$$

where I is the measured secondary ion current, plotted against the sputtering depth, x. The nominal depth resolution, Δx, associated to each point of the profile, was calculated, by analogy with Eq. (1), as the product between the sampling rate, $K\ I_p$, and the acquisition time, e.g., 2.5 s for $I_p = 2$ nA (short-range profiles) and 400 s for $I_p = 50$ nA (long-range profiles). Typical long-range and short-range depth profiles are shown in Fig. 5.

3. Theory

We assume that the quantity $c(x)$ is composed of two contributions: one is proportional to the amount of labelled water diffused – presumably in the form of $H_2{}^{18}O$ molecules, $^{18}O^{2-}$ and $^{18}OH^-$ ions, or more complex hydrogen–oxygen species [2,3] – along the grain boundaries between x and $x + \Delta x$; the other one comes from ^{18}O atoms which, after chemical reaction of water molecules with the UO_2 lattice, are incorporated and diffuse into the grains. This latter mechanism is often termed as "lattice" diffusion and

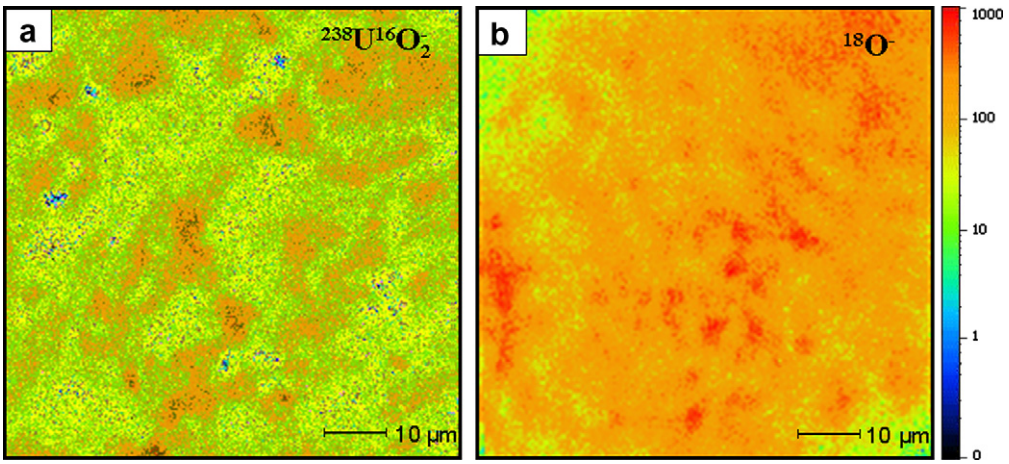

Fig. 2. (a) SIMS UO_2^- ion map of the surface of the pellet not exposed to labelled water. (b) $^{18}O^-$ ion maps of the leached pellet, showing an almost uniform oxidation of the sample surface. (For interpretation to colours in this figure, the reader is referred to the web version of this paper.)

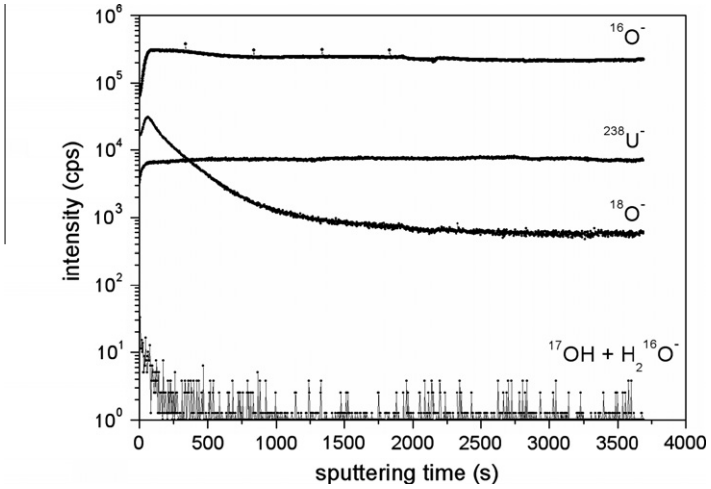

Fig. 3. SIMS raw data of shallow depth profiling for $^{16}O^-$, $^{18}O^-$, $^{238}U^-$, and $^{17}OH^- + H_2{}^{16}O^-$ (cumulative signal).

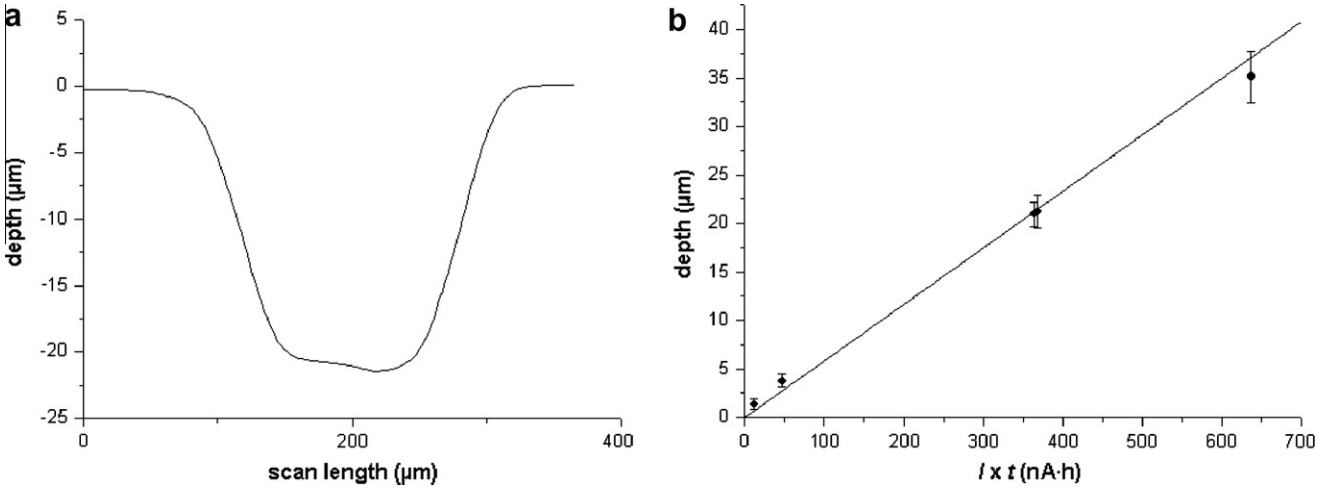

Fig. 4. (a) Profilometry of a typical SIMS crater for long-range diffusion investigation. (b) Plot of crater depths against the product of the sputtering time t and the primary intensity I: the slope of the linear fit represents the sputtering rate calibration factor.

proceeds through vacancies and interstitials according to Fick's second law.

An early idealization of grain boundary diffusion was provided by Fisher [13], who considered the grain boundary to be a thin layer of high-diffusivity material between two grains characterized by low bulk (i.e., lattice) diffusivity. The grains on either side are considered regular in shape (semi-infinite parallelepipeds) and large compared to the width of the grain boundary, δ, and to the

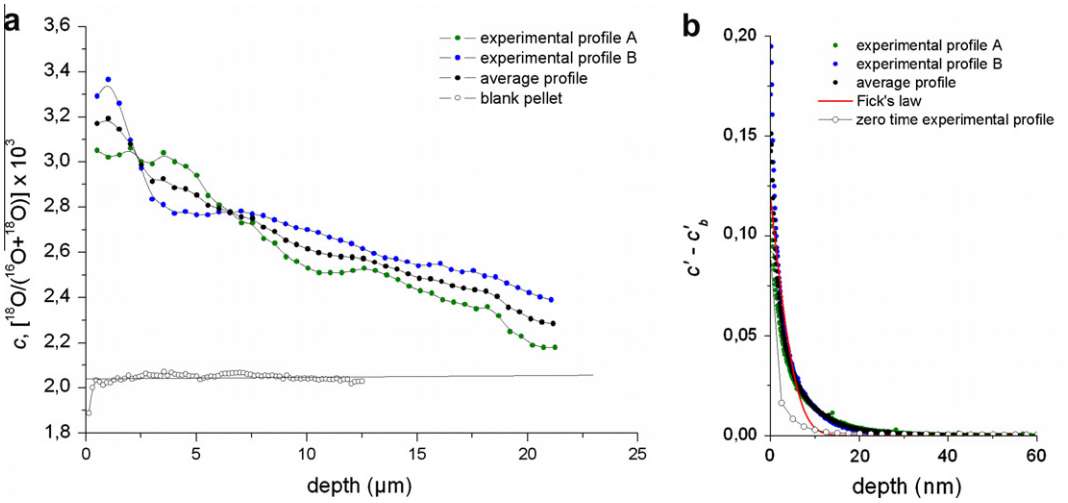

Fig. 5. (a) SIMS long-range profiles on the leached pellet (full points) and on the blank sample (open points); the reference oxygen isotopic ratio was measured by a linear fit of the blank profile (black straight line). (b) SIMS short-range diffusion profiles (full points), and fit of the average curve according to Eq. (11); a zero contact-time profile (open points) was acquired on the blank pellet immediately after superficial wetting.

distance, λ, over which the solute diffuses within the lattice during the time under consideration, t. Denoting by y the coordinate perpendicular to the grain boundary, and by D_B and D_L the diffusion coefficient along the grain boundary and the grain lattice, respectively, the diffusant concentration, $\xi(x, y, t)$, obeys the differential equation

$$\frac{\partial \xi}{\partial t} = D_B \frac{\partial^2 \xi}{\partial x^2} + \frac{2D_L}{\delta} \cdot \left.\frac{\partial \xi}{\partial y}\right|_{y=\delta/2} \tag{3}$$

in the boundary slab, and Fick's law

$$\frac{\partial \xi}{\partial t} = D_L \nabla^2 \xi \tag{4}$$

outside the grain boundary (note that the system is invariant in the z direction orthogonal to x and y). Indicating by $C(x, t)$ the mean value of $\xi(x, y, t)$ over a distance $y = 2L$ centred about the grain boundary, i.e., $C(x,t) \equiv \frac{1}{2L}\int_{-L}^{+L} \xi(x,y,t)dy$, it is straightforward to note that

$$C(x,t) \approx \frac{1}{2L}\int_{-\infty}^{+\infty} \xi(x,y,t)dy \tag{5}$$

for values of L of the order of or higher than the lattice diffusion length λ ($\lambda \equiv 2\sqrt{D_L t}$). Making use of Eq. (5), Fisher's main finding can be rewritten as

$$C(x,t) \propto \sqrt{t}\exp[-\alpha_F(t)x] \tag{6}$$

where $\alpha_F(t)$ is a factor depending also on the quantities δ, D_B and D_L. This result was derived under the boundary conditions that the diffusant concentration is held constant at the surface of the material and that $\xi(x, y, t)$ is continuous at the grain–grain boundary interface, as well as under a number of approximations [13].

The first exact solution of the coupled differential Eqs. (3) and (4) is due to Whipple [14]. He also assumed the above-mentioned boundary conditions, and used a Fourier–Laplace transform to obtain a solution in integral form. Furthermore, Whipple showed that an asymptotic approximation for $C(x, t)$ at large penetration depths is given by

$$C(x,t) \sim \exp\left[-\alpha_W(t)x^{4/3}\right] \tag{7}$$

where α_W is a time-dependent factor analogue to α_F.

Subsequently, Levine and MacCallum [15] generalized the Fisher–Whipple model to include diffusion from the specimen surface through the grains and diffusion around the grains through the boundaries. Their numerical analysis indicated that beneath a surface layer where $\partial \ln C/\partial(x^2)$ is constant due to direct lattice diffusion, there is a region where the slope $\alpha_{L-M} \equiv -\partial \ln C/\partial(x^{6/5})$ is constant, and the quantity δD_B can be obtained from the following equation [16]:

$$\delta D_B = 1.946\left(\frac{D_L}{t}\right)^{1/2}\alpha_{L-M}^{-5/3} \tag{8}$$

For our purposes, whether the Fisher's, Whipple's or Levine–MacCallum's model is used, the symmetry of the original formulation of the problem (i.e., ideal bi-crystal) and the spatial periodicity of an actual polycrystal allow us to immediately extend the functional form of the one-dimension-averaged quantity $C(x, t)$ to the surface-averaged quantity $c(x)$ we measured by SIMS in polycrystalline UO_2 after a certain diffusion time t.

Although Fisher's and Whipple's solutions have been widely used for the interpretation of experimental concentration–depth curves in a variety of diffusant/matrix systems, Levine and MacCallum's approach is regarded as the most appropriate for polycrystalline solids [17]. In particular, concerning the application of the Levine–MacCallum model to SIMS depth profiling, it is worth mentioning the work of Nagy and Giletti [2] on oxygen/water diffusion along lamellar boundaries in a macroperthitic feldspar, following hydrothermal exchange with ^{18}O-labelled water at 770–970 K, 1 kbar; the work of Fielitz et al. [18] on oxygen diffusion in polycrystalline mullite ceramics, following gas/solid exchange in an ^{18}O-enriched atmosphere at 1370–1600 K, 200 mbar; as well as the study of Sabioni et al. [8] on uranium self-diffusion in polycrystalline UO_2, following annealing in a ^{235}U-enriched UO_2 powder at 1770–1970 K. In our case, however, we decided to adopt a phenomenological approach to fit the long-range depth profiles, and made use of a generalized equation of the form

$$c(x) = c_\infty + (c_s - c_\infty)\exp(-\alpha x^n) \tag{9}$$

where c_∞ is the natural abundance of ^{18}O; c_s is the ^{18}O concentration at the surface, i.e., $c_s = c(0)$; n is an exponent which takes values according to the particular model under consideration (i.e., $n = 1$, 6/5 or 4/3 according to Fisher, Levine–MacCallum or Whipple, respectively); and α is a parameter with the same meaning of the factors α_F, α_W or α_{L-M}.

4. Results and discussion

The morphology of the polycrystalline UO_2 structure (blank pellet) as visible in the SEM image of Fig. 1 is recognizable also in the SIMS UO_2^- ion map of Fig. 2a, where the different intensities of the signal are due to the different crystallographic orientation of the grains. From the analysis of the $^{18}O^-$ ion map in Fig. 2b, we found no evidence of particular patterns of surface oxidation preferentially occurring along the grain boundaries.

Nevertheless, as shown in Fig. 5a, depth profiles acquired on the leached pellet at higher primary beam intensity (50 nA) and several hours of continuous sputtering, showed a deviation up to a depth of at least 22 μm from the natural $^{18}O/(^{16}O + ^{18}O)$ isotopic ratio measured on the non-leached pellet (2.0×10^{-3}, open points and related fit in Fig. 5a). This reveals a long-range, low-concentration (in the order of a few per mille, surface-averaged) "water" diffusion regime, and suggests that the grain boundaries, behaving as high-diffusivity-paths, are responsible for the penetration of the leachant up to such depths. Fig. 5b provides, on the contrary, a zoom of the near-surface region of the sample. As mentioned in Section 2, this region was probed with a lower primary beam current (2 nA), so that the first tens nm beneath the sample surface could be analysed with a higher depth resolution ($\Delta x = 0.1$ nm) compared to the long-range profile ($\Delta x = 500$ nm). The experimental curves (blue and green points[1]) show a high-concentration (in the order of 10%), short-range (<20 nm) profile. The quantity $(c' - c'_b)$ is actually plotted in this case, being $c'(x)$ the concentration in this near-surface region and $c'_b = 0.0032$ the background concentration. A "zero contact-time" profile ($t = 0$) was acquired on the blank pellet immediately after superficial wetting with labelled water and it is reported in Fig. 5b (open points) as a term of reference ($c'_b = 0.002$ in this case).

Notwithstanding surface roughness is comparable to or higher than the characteristic thickness of the near-surface region, a sputtered depth perpendicular to the normal of a surface element can however be defined according to Barber et al. [19]. The variation of this quantity by the effect of its dependence on the local angle of incidence of the ion beam can be neglected in our case, due to the low values of rugosity and roughness profile average slope we found on the sample surface. The local sputtered depth can then be considered homogeneous and topographically congruent all over the field of analysis of the ion beam, and calculated by analogy with Eq. (1). Taking also into account that $\Delta x \ll S_{RMS}$ in our measuring conditions, we associated this "effective" depth to the concentration profiles of Fig. 5b. Considering that the direction of the net diffusion flow is locally normal to the surface [20], and hence parallel to a sputtering "trajectory" [19,21], we finally argue that the short-range, long contact-time profiles are representative of ^{18}O lattice diffusion. The zero-time profile can instead provide an indication on the actual depth resolution. The evaluation of the actual depth resolution for SIMS shallow depth profiling is a complex matter, being this quantity affected by a number of factors (e.g., roughness and other surface effects), and depending on the depth itself. Roughly speaking, for our purposes the nominal depth resolution can be considered as the lower bound of the actual resolution, while the width of the zero-time profile (measured, for example, at 10% of its initial value) can be regarded as the upper bound. We can definitely state, therefore, that our actual depth resolution is in the order of 1 nm.

The overall frame just described matches the qualitative picture expected from diffusion experiments at low annealing temperatures, which typically show three recognizable regions [22]: a narrow superficial region characterized by direct lattice diffusion from the surface; a deeper transition region; the most penetrating "tail" due to grain boundaries diffusion. In what follows we have quantitatively verified this hypothesis.

The average profile of Fig. 5a is shown in Fig. 6 in terms of the normalized isotopic ratio $r(x) \equiv (c(x) - c_\infty)/(c_s - c_\infty)$. Except for the first two points, the experimental curve follows the straight line trend expected when Eq. (9) is represented as a power law (i.e., ln r vs. x) on a log–log plot. Eq. (9) was then fitted to this average depth profile imposing the three different values of n given by the approximated solutions of Fisher ($n = 1$) [13], Whipple ($n = 4/3$) [14] and Levine and MacCallum ($n = 6/5$) [15]. As shown in Fig. 6, all three models fit the data comparably well. While Fisher's solution seems to give the best fit in terms of χ^2 (Whipple's and Levine's fits give χ^2 that are respectively 1.5 and 2 times larger), we nevertheless relied on Levine–MacCallum's model in order to calculate the quantity δD_B by means of Eq. (8), as discussed in Section 3. The parameter α_{L-M} of Eq. (8) is now given by the fit with $n = 6/5$ and D_L can be derived from literature data via a room-temperature extrapolation of the Arrhenius plot at high temperature. According for example to Lay [4],

$$D_L = 0.5^{+2.0}_{-0.4} \cdot 10^{-4} \exp\left(-\frac{119,000 \pm 15,000}{RT}\right) \tag{10}$$

where R is the gas universal constant (8.314 J K^{-1} mol^{-1}) and T is the temperature in Kelvin. At 298 K the lattice diffusion coefficient of oxygen in UO_2 would be $D_L \approx 6.9 \times 10^{-26}$ m^2 s^{-1}.

Nevertheless, an estimate of D_L at the temperature investigated can also be obtained from the study of the thin near-surface region of the sample. Neglecting the impact of surface roughness and assuming direct lattice diffusion to be the main phenomenon governing the experimental profile in this region (while the contribution of grain boundary diffusion can be considered as a virtually constant background effect, here expressed by the term c'_b), the classic solution of Fick's law [20] can be used to fit the average curve in Fig. 5b:

$$c'(x) - c'_b = (c'_s - c'_b)\,erfc\left(\frac{x}{\lambda}\right) \tag{11}$$

where *erfc* is the complementary error function and the parameter λ is the lattice diffusion length already defined in Section 3. The quantity $(c'_s - c'_b)$ is treated as a free parameter due to the large variability of the surface concentration. Moreover, the first two points of the profile are precautionarily not taken into account by the fit, in order to minimize possible artefacts induced by the roughness

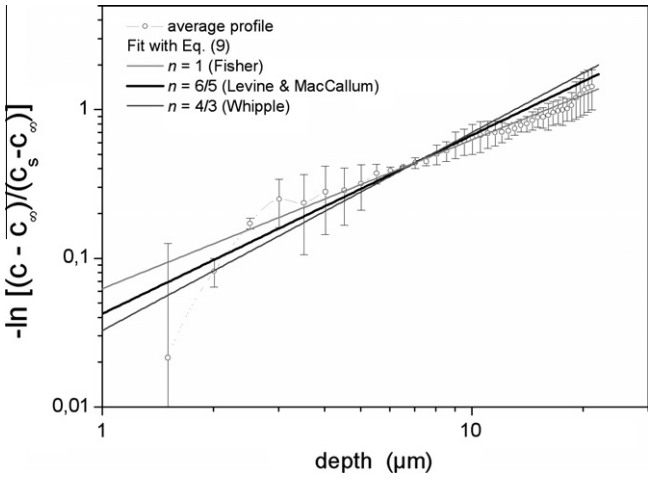

Fig. 6. Analysis of the long-range diffusion profile (from the average curve of Fig. 5a). Experimental points are fitted according to the functional form of Eq. (9).

[1] For interpretation of color in Fig. 5, the reader is referred to the web version of this article.

and the initial transient sputtering regime, as visible in the zero-time profile of Fig. 5b. As can be seen from Fig. 5b, this model fits well the steep descending edge of the profile but deviates from it at lower concentrations of tracer, i.e., at greater depths, where the effect of grain boundaries begins to be significant. From this fit, a diffusion length $\lambda \approx 6.6$ nm is obtained for oxygen after a leaching time of 3 months. This results in $D_L \approx 1.4 \times 10^{-24}$ m^2 s^{-1}.

With this value of D_L, and $\alpha_{L-M} = 8.5 \times 10^{-6}$ nm$^{-6/5}$ as given by the $n = 6/5$ fit in Fig. 6, we obtained $\delta D_B \approx 2.3 \times 10^{-25}$ m^3 s^{-1} from Eq. (8). As to the grain boundary width, a value of $\delta \approx 1$–2 nm is normally accepted as a reasonable estimate for ceramic materials and for UO_2 has been confirmed by Kubo et al. [23] via impedance measurements. Taking $\delta = 1$ nm, the grain boundary diffusion coefficient would be $D_B \approx 2.3 \times 10^{-16}$ m^2 s^{-1}.

It is now possible to verify *a posteriori* that the assumptions made when applying the high-diffusivity-paths model are fulfilled, and the values found for the diffusion coefficients are realistic. *In primis*, the applicability of the model essentially depends on the particular kinetic regime of grain boundary diffusion. Eq. (8) is valid for polycrystals in the so-called *type-B* kinetics regime, which, according to Harrison's conditions [24], is defined by the relation:

$$\delta < \sqrt{D_L t} \ll d \tag{12}$$

where d is the mean linear dimension of the grains. In our case, as mentioned above, it was found $d \approx 9$ μm, and $\sqrt{D_L t} \approx 3.3$ nm. Thereby the condition in Eq. (12) is evidently verified. Secondly, the 6/5-solution of Levine–MacCallum's model is derived under the condition

$$0.5 < \eta\tau^{-1/4} < 8 \tag{13}$$

where $\eta \equiv (x/\delta)(6D_L/D_B)^{1/2}$, $\tau \equiv 4D_L t/\delta^2$, and the quantity $\eta\tau^{-1/4}$ is referred to as an "effective" penetration depth [15]. With the values of D_L and D_B we obtained, Eq. (13) is fulfilled for $6.5 < x < 110$ μm, that is for penetration depths roughly equal to, or larger than, the mean diameter of the grains, as physically sound.

The value of D_L we have obtained is two orders of magnitude higher than the one given by Eq. (10) after Lay [4] for $T = 298$ K, and is affected by a large uncertainty owing to the unavoidable impact of surface roughness on SIMS shallow depth profiling. As already mentioned, Lay's findings were the result of a more indirect measurement approach and, moreover, were based on the Arrhenius fit of data obtained in the temperature range 900–1400 K. In fact, considering the uncertainties in Eq. (10), one can see how at $T = 298$ K the D_L value spans over seven orders of magnitude, i.e., between 3.3×10^{-29} and 1.1×10^{-22} m^2/s. Our estimate of D_L, however, is certainly compatible with the upper bound of Lay's value.

The same drawback in the room-temperature extrapolation of high-temperature Arrhenius plots persists when the results of Sabioni et al. [8] are taken into consideration (temperature in the range 880–1000 K). Moreover, the profiles reported in this latter work show quite an unrealistic uptake of ^{18}O by the UO_2 matrix (both polycrystal and single crystal), considering a concentration of $H_2{}^{18}O$ in the vapour atmosphere lower than 0.25% in volume and short exposure times (10^3–10^4 s), which raises some doubts regarding the diffusion coefficients derived from those data.

Furthermore, the analysis made by Sabioni et al. [8] shows similar diffusion profiles for single-crystal and polycrystalline UO_2, and takes this similarity as evidence of simple lattice diffusion, stating that grain boundaries are not preferential paths for oxygen diffusion in UO_2. It is worth noting that the value of $D_L = 3.61 \times 10^{-16}$ m^2 s^{-1} there reported (for an exposure time of 1860 s at 1000 K) corresponds to a diffusion length of about 1.6 μm, while the study only shows diffusion profiles up to 4 μm. Thus, it is not surprising that the profiles for single-crystal and polycrystalline UO_2 shown in their article do not appreciably diverge. In fact, the depth of 4 μm probed is of the same order as the diffusion length of oxygen in the lattice and smaller than the grain size, 12 μm. The typical tail of grain boundary diffusion – for which moreover we measure an ^{18}O isotopic abundance two orders of magnitude smaller than the one on the surface – would have been visible only if greater depths had been investigated and an isotopic intensity scale of the same order of magnitude of the ^{18}O natural abundance had been adopted.

5. Conclusions

The values of the diffusion coefficients of oxygen in the lattice, $D_L \approx 1.4 \times 10^{-24}$ m^2 s^{-1}, and of water species along the grain boundaries, $D_B \approx 2.3 \times 10^{-16}$ m^2 s^{-1}, estimated from the above described SIMS analysis, are judged to be realistic. In fact, the kinetics conditions for which the high-diffusivity-paths model is valid are fulfilled, and the values of the diffusion coefficients are not far from those that can be extrapolated from literature data obtained at higher temperatures, especially if the errors implicit in the Arrhenius plot extrapolation are taken into account.

Temperature has in fact a crucial influence on the value of the diffusion coefficient, and at the same time represents a limiting factor from the experimental point of view, since the diffusion length at lower temperatures becomes more difficult to determine. In this respect, SIMS is possibly the most powerful tool for this sort of application, as it can guarantee a direct observation of the short-range diffusion with a nanometre resolution. Furthermore, despite the difficulties related to SIMS diffusion studies at large penetration depths (due to very long measurement times in stable sputtering conditions and to crater-edge effects), it was possible to evaluate also low-concentration, long-range diffusion of water species up to 22 μm.

Evidently, the study of UO_2 single crystals – a matrix void of grain boundaries – is necessary for a direct evaluation of the lattice diffusion coefficient, and this is an important short-term objective we plan to address. Our findings, although preliminary, nevertheless give a glimpse of the potentiality for further studies of the methodology we have applied here. Among other things, the role and impact of oxygen/water-species diffusion coefficients in spent fuel long-term oxidation kinetics can clearly be seen by reversing the mathematical approach we have utilized to retrieve D_B. In fact, assuming pellet stoichiometry is locally correlated to the concentration of diffused oxygen/oxidant species, the use of Levine–MacCallum's model along with the experimentally determined diffusion coefficients can straightforwardly show how matrix stoichiometry – averaged over a circular crown – will evolve as a function of contact time with water and of distance from the pellet edge. More importantly, obtaining reliable data for oxygen diffusion in UO_2 can substantiate the expected correlation between oxygen diffusion and radionuclides release in aqueous solution [25]. This will help develop models for the reaction behaviour of spent fuel in contact with groundwater, and therefore predict fuel long-term stability and durability.

Acknowledgments

We would like to gratefully thank E. Maugeri and T. Wiss for the SEM characterization of polycrystalline UO_2, as well as F. Heberling and E. Bohnert for the AFM analysis. Our acknowledgement also goes to V.V. Rondinella, C. Walker, V. Oversby and J.-P. Glatz for fruitful discussions. I.M. gratefully acknowledges the European Commission for funding her research fellowship at the Institute for Transuranium Elements, Karlsruhe, Germany.

References

[1] W.J. Weber, R.C. Ewing, C.R.A. Catlow, T. Diaz de la Rubia, L.W. Hobbs, C. Kinoshita, Hj. Matzke, A.T. Motta, M. Nastasi, E.H.K. Salje, E.R. Vance, S.J. Zinkle, J. Mater. Res. 13 (1998) 1434–1484.

[2] K.L. Nagy, B.J. Giletti, Geochim. Cosmochim. Acta 50 (1986) 1151–1158.
[3] A. Matthews, J. Goldsmith, R. Clayton, Geol. Soc. Amer. Bull. 94 (1983) 396–412.
[4] K.W. Lay, J. Am. Ceram. Soc. 53 (1970) 369–373.
[5] J.T. Bittel, L.H. Sjodahl, J.F. White, J. Am. Ceram. Soc. 52 (1969) 446–451.
[6] J. Belle, J. Nucl. Mater. 30 (1969) 3–15.
[7] SKI Technical Report 96:36, Swedish Nuclear Power Inspectorate, Stockholm, 1996, pp. 265–266.
[8] A.C.S. Sabioni, W.B. Ferraz, F. Millot, J. Nucl. Mater. 278 (2000) 364–369.
[9] E. Maugeri, Helium Behaviour in UO_2 Under Conditions Relevant for Spent Fuel Storage, PhD Thesis, University of Pavia, 2009.
[10] I. Horcas, R. Fernández, J.M. Gómez-Rodríguez, J. Colchero, J. Gómez-Herrero, A.M. Baro, Rev. Sci. Instrum. 78 (2007) 013705.
[11] A.D. McNaught, A. Wilkinson, IUPAC Compendium of Chemical Terminology, second ed., The Gold Book, Blackwell Scientific Publications, Oxford, 1997.
[12] L. Desgranges, B. Pasquet, Nucl. Instrum. Methods Phys. Res., Sect. B 215 (2004) 545–551.
[13] J.C. Fisher, J. Appl. Phys. 22 (1951) 74–77.
[14] R.T.P. Whipple, Philos. Mag. 45 (1954) 1225–1236.
[15] H.S. Levine, C.J. MacCallum, J. Appl. Phys. 31 (1960) 595–599.
[16] P.G. Shewmon, Diffusion in Solids, second ed., The Minerals Metals and Materials Society, Warrendale, 1989. pp. 189–205.
[17] I. Kaur, Y. Mishin, W. Gust, Fundamentals of Grain and Interphase Boundary Diffusion, third ed., Wiley and Sons, Chichester, 1995.
[18] P. Fielitz, G. Borchardt, M. Schmücker, H. Schneider, P. Willich, J. Am. Ceram. Soc. 87 (2004) 2232–2236.
[19] D.J. Barber, F.C. Frank, M. Moss, J.W. Steeds, I.S.T. Tsong, H.H. Wills, J. Mater. Sci. 8 (1973) 1030.
[20] J. Cranck, The Mathematics of Diffusion, second ed., Oxford University Press, Oxford, 1975. pp. 28–43.
[21] A. Benninghoven, F.G. Rüdenhauer, H.W. Werner, Secondary Ion Mass Spectrometry, Chemical Analysis, vol. 86, Wiley Interscience, New York, 1987.
[22] Y. Mishin, Phys. Status Solidi (a) 129 (1992) 101–116.
[23] T. Kubo, S. Ishimoto, T. Koyama, J. Nucl. Sci. Technol. 30 (1993) 664–672.
[24] L.G. Harrison, Trans. Faraday Soc. 57 (1961) 1191–1199.
[25] B. Grambow, Spent Fuel Dissolution and Oxidation, an Evaluation of Literature Data, SKB Technical Report TR-89-13, Stockholm, 1989.